2019 IEEE 58th Conference on Decision and Control (CDC)
Palais des Congrès et des Expositions Nice Acropolis
Nice, France, December 11-13, 2019

On Impact De-orbiting for Satellites Using a Prescribed Impedance Behavior*

Kostas Nanos, Foteini Xydi-Chrysafi, and Evangelos Papadopoulos, *Fellow, IEEE*

Abstract— **In a number of on-orbit applications, such as de-orbiting, continuous contact between a servicing robot (chaser) and a serviced satellite (target) is needed. The task includes chaser free-space motion and subsequent contact interaction with a floating target. To achieve this, usually grasping of the satellite is proposed. However, most of the existing satellites on orbit have no dedicated grapple fixtures. In this paper, the problem of continuous contact between two bodies lacking a rigid grasp and fixed bases is studied. It is shown that continuous contact can be achieved by setting an appropriate chaser velocity at the moment of contact, accompanied by an impedance controller. The same controller is applied in both phases without switching, avoiding loss of contact and instabilities, due to unavoidable transition delays and unknown properties. A methodology is developed for selecting the same controller parameters and a suitable trajectory during both phases. The method is valid for spatial systems and illustrated by a planar example.**

I. Introduction

The interaction of a robotic manipulator with its environment is important in many applications. To obtain a desired response and limit contact oscillations, interactions require an appropriate control method. In space, contact interactions are important in tasks such as satellite de-orbiting during which the manipulator of a servicer satellite (chaser) comes into contact with a satellite (target), aiming at target reentry or de-orbiting [1], see Fig. 1.

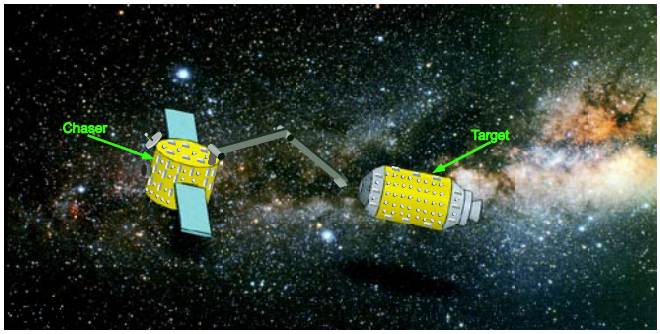

Fig. 1. A satellite (target) deorbiting by a robotic chaser.

These tasks require continuous contact between the chaser and the target; else the target may drift from its desired trajectory. Impedance controllers are natural candidates for such interactions. To regulate the relationship between end-effector velocity and force during a dynamic interaction of a single manipulator, Hogan proposed impedance control [2]. Subsequently, many researchers have dealt with impedance control applied to a number of tasks. Many researchers have extended the approach of impedance control to robotic space manipulator systems on-orbit. Yoshida et al. have proposed the concept of impedance matching and studied whether the contact with the target is maintained or lost and the target pushed away [3]. The virtual mass concept for using impedance control on orbit has been proposed, aiming to represent the influence of the end-effector impedance on the target motion [4]. To manipulate an object by multi-arm robotic systems on orbit, the Multiple Impedance Control (MIC) has been developed [5], which exploits the Object Impedance Control (OIC) [6].

Many research works study the capture of free-floating satellites by grasping them from a grapple fixture. Abiko et al. studied an impedance controller for a free-floating space robot during grasping of a tumbling target with model uncertainty [7]. A method for validation of the robotic subsystem during chaser rendezvous and grasping manoeuvre has been developed using microgravity simulators [8]. Lampariello et al. have presented a novel method for grasping a partially cooperative tumbling satellite with a free-floating robot. An extended Kalman filter was implemented for providing robustness and a velocity estimate of the tumbling satellite as a feed-forward for control, throughout the grasping task [9]. To minimize interaction forces between a robot manipulator and a satellite while maintaining contact, Sharma et al. proposed an approach based on direct force control in the presence of a rigid grasp [10]. However, the proposed design requires controller switching between the free-space and the contact phase. The online path planning and compliance control of space robot for capturing a rotating object is studied in [11]. An impedance control scheme has been proposed in [12] and more recently in [13], so that the servicer robot and the target satellite have the same velocity after the contact. However, in both works, only the contact phase is studied, and the proposed controllers are designed considering a non-oscillating response during the impact.

In this paper, the problem of maintaining continuous contact without a grasp between a chaser and its target is studied. The task is divided in the free-space and the contact phases. It is shown, that continuous contact between two moving bodies is achieved by the selection of an appropriate chaser velocity at the moment of contact, accompanied by an impedance controller. A methodology is developed for selecting

* Support by the H2020 Operational Grant n°7 – EROSS, funded by the European Commission under Grant Agreement #821904 is acknowledged.
Kostas Nanos, Foteini Xydi-Chrysafi and Evangelos Papadopoulos are with the School of Mechanical Engineering, National Technical University of Athens, Greece (phone: +30-210-772-1440; fax: +30-210-772-1450; e-mail: {nanos.kostas, fotini09xydi}@gmail.com, egpapado@central.ntua.gr).

controller parameters and a trajectory for a desired response during both phases. The application of the method is valid for spatial systems and is illustrated by a planar example.

II. System Dynamics

A space manipulator system (chaser) on-orbit consists of a manipulator mounted on a spacecraft equipped with actuators such as thrusters and reaction wheels. According to the current practice in space, the chaser's manipulator has revolute joints and an open chain kinematic configuration, so that, in a system with an N degree-of-freedom (DoF) manipulator, there will be $N+6$ DoF in total.

During the contact phase, external forces $\mathbf{F}_{\mathbf{ext}}$ and moments $\mathbf{n}_{\mathbf{ext}}$ act on both the chaser's end-effector and the free-floating object (target). In this case, the equations of motion of the target are given by

$$\mathbf{F}_{\mathbf{ext}} = m_t \ddot{\mathbf{r}}_{\mathbf{t}} \tag{1}$$

and

$$\mathbf{n}_{\mathbf{ext}} = \mathbf{I}_{\mathbf{t}}\dot{\boldsymbol{\omega}}_{\mathbf{t}} + \boldsymbol{\omega}_{\mathbf{t}} \times (\mathbf{I}_{\mathbf{t}} \times \boldsymbol{\omega}_{\mathbf{t}}) \tag{2}$$

where m_t and $\mathbf{I}_{\mathbf{t}}$ is the target mass and moment of inertia matrix, respectively. Furthermore, $\boldsymbol{\omega}_{\mathbf{t}}$ and $\mathbf{r}_{\mathbf{t}}$ is the target angular velocity and the position vector of its center of mass (CoM) with respect to the inertial frame, respectively.

The equation of motion of the chaser robot is given by

$$\mathbf{H}(\boldsymbol{\delta}_{\mathbf{0}},\mathbf{q})\ddot{\mathbf{z}} + \mathbf{c}(\boldsymbol{\delta}_{\mathbf{0}},\mathbf{q},\dot{\boldsymbol{\delta}}_{\mathbf{0}},\dot{\mathbf{q}}) = \mathbf{Q}_{\mathbf{act}} - \mathbf{Q}_{\mathbf{ext}} \tag{3}$$

where $\mathbf{c}$ is the vector of the nonlinear Coriolis and centrifugal terms and

$$\mathbf{z} = \left[\mathbf{r}_{\mathbf{C}_0}{}^T \;\; \boldsymbol{\delta}_{\mathbf{0}}{}^T \;\; \mathbf{q}^T\right]^T \tag{4}$$

where $\mathbf{r}_{\mathbf{C}_0}$ is the position vector of the chaser's spacecraft CoM with respect to the inertial frame, $\boldsymbol{\delta}_{\mathbf{0}}$ the column vector of a set of Euler angles describing the spacecraft attitude and $\mathbf{q}$ the column vector of the manipulator joint angles.

The $(6+N)\times(6+N)$ matrix $\mathbf{H}(\mathbf{q},\boldsymbol{\delta}_{\mathbf{0}})$ is given by

$$\mathbf{H}(\mathbf{q},\boldsymbol{\delta}_{\mathbf{0}}) = \tilde{\mathbf{E}}^T(\boldsymbol{\delta}_{\mathbf{0}})\tilde{\mathbf{H}}(\mathbf{q})\tilde{\mathbf{E}}(\boldsymbol{\delta}_{\mathbf{0}}) \tag{5}$$

where $\tilde{\mathbf{H}}(\mathbf{q})$ is the system inertia matrix and

$$\tilde{\mathbf{E}}(\boldsymbol{\delta}_{\mathbf{0}}) = \begin{bmatrix} \mathbf{I}_{3\times3} & \mathbf{0}_{3\times3} & \mathbf{0}_{3\times N} \\ \mathbf{0}_{3\times3} & \mathbf{E}(\boldsymbol{\delta}_{\mathbf{0}})_{3\times3} & \mathbf{0}_{3\times N} \\ \mathbf{0}_{N\times3} & \mathbf{0}_{N\times3} & \mathbf{I}_{N\times N} \end{bmatrix} \tag{6}$$

where $\mathbf{I}_{\mathbf{k}\times\mathbf{k}}$ is the $k\times k$ unity matrix, $\mathbf{0}_{\mathbf{m}\times\mathbf{n}}$ is the $m\times n$ zero matrix and $\mathbf{E}(\boldsymbol{\delta}_{\mathbf{0}})$ is a 3×3 matrix which relates the spacecraft angular velocity $\boldsymbol{\omega}_{\mathbf{0}}$ to the Euler rates $\dot{\boldsymbol{\delta}}_{\mathbf{0}}$.

The generalized forces $\mathbf{Q}_{\mathbf{act}}$ and $\mathbf{Q}_{\mathbf{ext}}$ which correspond to the actuator forces/torques $\mathbf{F}_{\mathbf{s}}/\mathbf{n}_{\mathbf{s}}$ applied to the spacecraft CoM and the torques $\boldsymbol{\tau}$ applied to the joints and the external forces/torques $\mathbf{F}_{\mathbf{ext}}/\mathbf{n}_{\mathbf{ext}}$ applied on the end-effector, respectively, arise from the principle of virtual work as follows

$$\delta W = \boldsymbol{\tau}^T\delta\mathbf{q} - \left[\mathbf{F}_{\mathbf{ext}}^T \;\; \mathbf{n}_{\mathbf{ext}}^T\right]\begin{bmatrix}\delta\mathbf{r}_{\mathbf{E}} \\ \hat{\mathbf{k}}\delta\theta_{\mathrm{E}}\end{bmatrix} + \left[\mathbf{F}_{\mathbf{s}}^T \;\; \mathbf{n}_{\mathbf{s}}^T\right]\begin{bmatrix}\delta\mathbf{r}_{\mathbf{C}_0} \\ \hat{\mathbf{a}}\delta\theta_0\end{bmatrix} \tag{7}$$

where $\mathbf{r}_{\mathbf{E}}$ is the position of the end-effector with respect to the inertial frame, the angles θ_0 and θ_{E} represent the spacecraft and end-effector orientation, respectively, and $\hat{\mathbf{a}}$, $\hat{\mathbf{k}}$ are the unit vectors in the direction of the spacecraft and end-effector angular velocity, respectively.

The corresponding virtual displacements are

$$\begin{bmatrix}\delta\mathbf{r}_{\mathbf{C}_0} \\ \hat{\mathbf{a}}\delta\theta_0\end{bmatrix} = \mathbf{J}_{\mathbf{s}}\begin{bmatrix}\delta\mathbf{r}_{\mathbf{C}_0} \\ \delta(\boldsymbol{\delta}_{\mathbf{0}}) \\ \delta\mathbf{q}\end{bmatrix}, \quad \begin{bmatrix}\delta\mathbf{r}_{\mathbf{E}} \\ \hat{\mathbf{k}}\delta\theta_{\mathrm{E}}\end{bmatrix} = \mathbf{J}_{\mathbf{v}}\begin{bmatrix}\delta\mathbf{r}_{\mathbf{C}_0} \\ \delta(\boldsymbol{\delta}_{\mathbf{0}}) \\ \delta\mathbf{q}\end{bmatrix} \tag{8}$$

where $\mathbf{J}_{\mathbf{v}}$ and $\mathbf{J}_{\mathbf{s}}$ are appropriate Jacobian matrices.

The combination of (7)-(8) yields

$$\delta W = (\mathbf{Q}_{\mathbf{act}} - \mathbf{Q}_{\mathbf{ext}})^T\begin{bmatrix}\delta\mathbf{r}_{\mathbf{C}_0} \\ \hat{\mathbf{a}}\delta\theta_0 \\ \delta\mathbf{q}\end{bmatrix} \tag{9}$$

where

$$\mathbf{Q}_{\mathbf{ext}} = \mathbf{J}_{\mathbf{v}}^T\begin{bmatrix}\mathbf{F}_{\mathbf{ext}} \\ \mathbf{n}_{\mathbf{ext}}\end{bmatrix} = \mathbf{J}_{\mathbf{v}}^T\boldsymbol{F}_{\mathbf{ext}} \tag{10}$$

and

$$\mathbf{Q}_{\mathbf{act}} = \begin{bmatrix}\mathbf{0}_{6\times1} \\ \boldsymbol{\tau}\end{bmatrix} + \mathbf{J}_{\mathbf{s}}^T\begin{bmatrix}\mathbf{F}_{\mathbf{s}} \\ \mathbf{n}_{\mathbf{s}}\end{bmatrix} = \mathbf{J}_{\mathbf{q}}\left[\mathbf{F}_{\mathbf{s}}{}^T \;\; \mathbf{n}_{\mathbf{s}}{}^T \;\; \boldsymbol{\tau}^T\right]^T \tag{11}$$

where $\mathbf{J}_{\mathbf{q}}$ appropriate matrix.

III. De-orbiting Impedance Control

This work aims at de-orbiting a satellite by contact despite the lack of a rigid grasp. It is assumed that the target satellite is partially cooperative and hence that its attitude is controlled. During a de-orbiting task, the chaser approaches the target satellite, which is floating freely in space, and after the contact, directs it for re-entry. Given that both the chaser and the target lack fixed bases, this task is very challenging. An important question that arises is whether a control strategy exists that will ensure that the two bodies will remain in contact throughout the task; if the contact is lost, the target will move in an uncontrolled way, and de-orbiting may fail. Moreover, in impacts where a high stiffness is involved, the target satellite might bounce away before the chaser controller has time to react, due to intrinsic time delays. To avoid hard impacts and increase contact duration of the impact, a passive compliant element of known structural properties is introduced at the chaser's end-effector, [12]. Hence, the contact phenomenon can be described by the wrist parameters since the wrist's compliance is usually chosen so that the wrist is the most compliant element in a system.

The concept is illustrated in Fig. 2. First, the chaser's end-effector is driven from its initial position to the target, Fig. 2(a). The contact between the two bodies is modeled by a generalized spring of stiffness $\mathbf{K}_{\mathbf{e}}$. The direction of the force is chosen such that it minimizes attitude disturbances. Fig. 2(b) shows the beginning of the contact when the interaction force $\mathbf{F}_{\mathbf{ext}}$ is still zero. In Fig. 2(c), contact has been achieved and the developed $\mathbf{F}_{\mathbf{ext}}$ causes target motion. Our interest here is to develop an appropriate control algorithm, select its parameters, and study the initial conditions needed to keep the two bodies in contact throughout the process.

The developed controller is derived considering that an equivalent force/torque $\boldsymbol{F}_{\mathbf{act}}$ acts on the end-effector which has the same effect as that due to the forces/torques $\mathbf{F}_s/\mathbf{n}_s$ applied on the spacecraft by thrusters and momentum devices, and the torques $\boldsymbol{\tau}$ applied by manipulator joint motors,

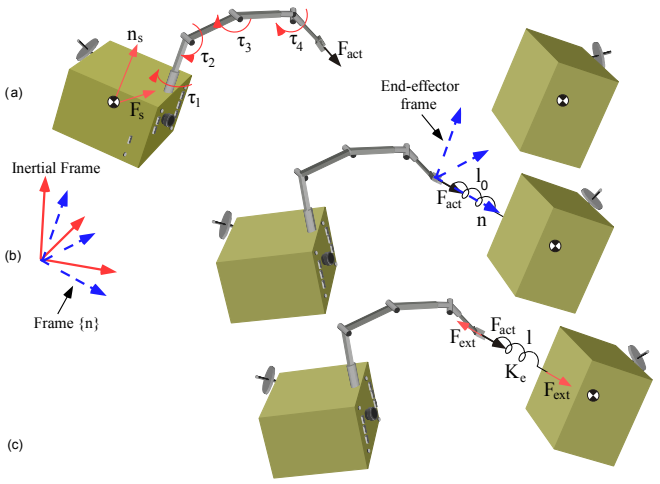

Fig. 2. (a) The chaser free motion, (b) the beginning of the contact and (c) the contact phase.

$$\boldsymbol{F}_{\mathbf{act}} = \begin{bmatrix} \mathbf{F}_{\mathbf{act}}^T & \mathbf{n}_{\mathbf{act}}^T \end{bmatrix}^T \tag{12}$$

In this case, the principle of virtual work yields:

$$\delta W = \left(\begin{bmatrix} \mathbf{F}_{\mathbf{act}}^T & \mathbf{n}_{\mathbf{act}}^T \end{bmatrix} - \begin{bmatrix} \mathbf{F}_{\mathbf{ext}}^T & \mathbf{n}_{\mathbf{ext}}^T \end{bmatrix} \right) \begin{bmatrix} \delta \mathbf{r}_{\mathbf{E}} \\ \hat{\mathbf{k}} \delta \theta_{\mathbf{E}} \end{bmatrix} \tag{13}$$

Using (8), one can write (13) in the form of (9), where $\mathbf{Q}_{\mathbf{ext}}$ is given by (10) and $\mathbf{Q}_{\mathbf{act}}$ is

$$\mathbf{Q}_{\mathbf{act}} = \mathbf{J}_{\mathbf{v}}^T \begin{bmatrix} \mathbf{F}_{\mathbf{act}} \\ \mathbf{n}_{\mathbf{act}} \end{bmatrix} = \mathbf{J}_{\mathbf{v}}^T \boldsymbol{F}_{\mathbf{act}} \tag{14}$$

Therefore, (3) can be written as

$$\mathbf{H}(\mathbf{q}, \boldsymbol{\delta}_0) \ddot{\mathbf{z}} + \mathbf{c}(\mathbf{z}, \dot{\mathbf{z}}) = \mathbf{J}_{\mathbf{v}}^T (\boldsymbol{F}_{\mathbf{act}} - \boldsymbol{F}_{\mathbf{ext}}) \tag{15}$$

Assuming the inertia matrix $\mathbf{H}(\mathbf{q}, \boldsymbol{\delta}_0)$ is non-singular, (15) can be written as

$$\ddot{\mathbf{z}} = \mathbf{H}^{-1}(\mathbf{q}, \boldsymbol{\delta}_0) \left(\mathbf{J}_{\mathbf{v}}^T (\boldsymbol{F}_{\mathbf{act}} - \boldsymbol{F}_{\mathbf{ext}}) - \mathbf{c}(\mathbf{z}, \dot{\mathbf{z}}) \right) \tag{16}$$

The end-effector's velocity is given by

$$\dot{\mathbf{x}} = \begin{bmatrix} \dot{\mathbf{r}}_{\mathbf{E}} \\ \dot{\boldsymbol{\delta}}_{\mathbf{E}} \end{bmatrix} = \mathbf{J}_{\mathbf{r}} \begin{bmatrix} \dot{\mathbf{r}}_{\mathbf{c}_0} \\ \dot{\boldsymbol{\delta}}_0 \\ \dot{\mathbf{q}} \end{bmatrix} = \mathbf{J}_{\mathbf{r}} \dot{\mathbf{z}} \tag{17}$$

where $\boldsymbol{\delta}_{\mathbf{E}}$ is a set of Euler angles describing the end-effector's orientation and $\mathbf{J}_{\mathbf{r}}$ is a Jacobian matrix.

Differentiating (17), yields the end-effector acceleration as

$$\ddot{\mathbf{x}} = \mathbf{J}_{\mathbf{r}} \ddot{\mathbf{z}} + \dot{\mathbf{J}}_{\mathbf{r}} \dot{\mathbf{z}} \tag{18}$$

Considering that the acceleration $\ddot{\mathbf{z}}$ is given by (16), the end-effector acceleration can be written as

$$\ddot{\mathbf{x}} = \mathbf{W}(\boldsymbol{F}_{\mathbf{act}} - \boldsymbol{F}_{\mathbf{ext}}) - \mathbf{J}_{\mathbf{r}} \mathbf{H}^{-1} \mathbf{c} + \dot{\mathbf{J}}_{\mathbf{r}} \dot{\mathbf{z}} \tag{19}$$

where the 6×6 matrix $\mathbf{W}$ is given by

$$\mathbf{W} = \mathbf{J}_{\mathbf{r}} \mathbf{H}^{-1} \mathbf{J}_{\mathbf{v}}^T \tag{20}$$

It is desired to govern the translational and attitude dynamics of the closed-loop system according to the impedance law

$$\mathbf{M}_{\mathbf{d}} \ddot{\mathbf{e}} + \mathbf{B}_{\mathbf{d}} \dot{\mathbf{e}} + \mathbf{K}_{\mathbf{d}} \mathbf{e} = -\mathbf{F}_{\mathbf{ext}} + \mathbf{F}_{\mathbf{des}} \tag{21}$$

where $\mathbf{F}_{\mathbf{des}}$ is a desired force introduced to obtain non-zero steady state forces during the contact, $\mathbf{M}_{\mathbf{d}}$, $\mathbf{B}_{\mathbf{d}}$ and $\mathbf{K}_{\mathbf{d}}$ are impedance gain matrices, and $\mathbf{e}$ is the chaser's end-effector position/orientation error, defined as

$$\mathbf{e} = \mathbf{x} - \mathbf{x}_{\mathbf{d}} \tag{22}$$

where $\mathbf{x}_{\mathbf{d}}$ is the desired end-effector's trajectory.

Therefore, the chaser end-effector acceleration is given by

$$\ddot{\mathbf{x}} = \mathbf{M}_{\mathbf{d}}^{-1} (-\boldsymbol{F}_{\mathbf{ext}} + \boldsymbol{F}_{\mathbf{des}} - \mathbf{B}_{\mathbf{d}} \dot{\mathbf{e}} - \mathbf{K}_{\mathbf{d}} \mathbf{e}) + \ddot{\mathbf{x}}_{\mathbf{d}} \tag{23}$$

Assuming $\mathbf{W}$ is non-singular, the combination of (19) and (23) results in the following control law

$$\begin{aligned} \boldsymbol{F}_{\mathbf{act}} = & (\mathbf{I}_{6\times6} - \mathbf{W}^{-1} \mathbf{M}_{\mathbf{d}}^{-1}) \boldsymbol{F}_{\mathbf{ext}} + \mathbf{W}^{-1} (\mathbf{J}_{\mathbf{r}} \mathbf{H}^{-1} \mathbf{c} - \dot{\mathbf{J}}_{\mathbf{r}} \dot{\mathbf{z}}) \\ & + \mathbf{W}^{-1} \mathbf{M}_{\mathbf{d}}^{-1} (\boldsymbol{F}_{\mathbf{des}} - \mathbf{B}_{\mathbf{d}} \dot{\mathbf{e}} - \mathbf{K}_{\mathbf{d}} \mathbf{e}) + \mathbf{W}^{-1} \ddot{\mathbf{x}}_{\mathbf{d}} \end{aligned} \tag{24}$$

where all the feedback variables can be measured by appropriate sensors.

Using (11) and (14), the actuator inputs are computed by

$$\begin{bmatrix} \mathbf{F}_{\mathbf{s}} \\ \mathbf{n}_{\mathbf{s}} \\ \boldsymbol{\tau} \end{bmatrix} = \mathbf{J}_{\mathbf{q}}^{-1} \mathbf{J}_{\mathbf{v}}^T \boldsymbol{F}_{\mathbf{act}} \tag{25}$$

Next, a systematic methodology of defining the impedance parameters $\mathbf{M}_{\mathbf{d}}$, $\mathbf{B}_{\mathbf{d}}$, $\mathbf{K}_{\mathbf{d}}$ and $\mathbf{F}_{\mathbf{des}}$ is developed so that the chaser will track the desired trajectory in the free-space phase and will not lose the contact with the target in the contact phase avoiding controller switching between the two phases.

IV. Controller Parameter Selection

The developed impedance control law, given by (24) is applied in both free-space and contact phases, and the necessary conditions are developed so that the same controller parameters are employed in both phases. In the following analysis, the variables with the subscripts ''f and c'' correspond to *free-space phase* and *contact phase*, respectively.

A. Free-Space Phase

In the free-space phase, see Fig. 2(a), no external force acts on the chaser ($\boldsymbol{F}_{ext} = \mathbf{0}$); the chaser's end-effector moves towards the target, following a desired trajectory $\mathbf{x}_{\mathbf{d,f}}(t)$. For this phase, the desired impedance law is

$$\mathbf{M}_{\mathbf{d}} \ddot{\mathbf{e}}_{\mathbf{f}} + \mathbf{B}_{\mathbf{d}} \dot{\mathbf{e}}_{\mathbf{f}} + \mathbf{K}_{\mathbf{d}} \mathbf{e}_{\mathbf{f}} = \mathbf{0} \tag{26}$$

where

$$\mathbf{e}_{\mathbf{f}} = \mathbf{x} - \mathbf{x}_{\mathbf{d,f}} \tag{27}$$

Each component (translational or rotational) $x_{d,f}(t)$ of the desired trajectory $\mathbf{x}_{\mathbf{d,f}}(t)$ during free-space phase is given by

$$x_{d,f}(t) = x_{ch,in} + s(t)(x_{ch,c} - x_{ch,in}) \tag{28}$$

where $x_{ch,in}$ is the initial trajectory component state of the chaser's end-effector in free-space phase, $x_{ch,c}$ is the corresponding chaser's end-effector trajectory component at the moment of contact, and $s(t)$ is a cubic or higher-order polynomial called the arc length parameterization of the path.

The chaser's end-effector position/orientation error transient response in the free-space phase is defined by the selection of the damping coefficient ζ_f and the natural frequency $\omega_{n,f}$ characterizing a desired second order response. Therefore, the diagonal elements m_d, and b_d of the diagonal matrices $\mathbf{M}_{\mathbf{d}}$ and $\mathbf{B}_{\mathbf{d}}$ are defined by the desired ζ_f and $\omega_{n,f}$ as

$$m_d = k_d / \omega_{n,f}^2 \tag{29}$$

$$b_d = 2\zeta_f \omega_{n,f} m_d \tag{30}$$

where the diagonal element k_d of the diagonal matrix $\mathbf{K}_{\mathbf{d}}$ can take an arbitrary and finite positive value.

B. Contact Phase

During the contact phase, the chaser's end-effector and the target move together, maintaining their contact, while an external force/torque $\boldsymbol{F}_{ext}$ is developed.

During the contact, it is desired that the error response is governed by the following impedance behavior

$$\mathbf{M_d}\,\ddot{\mathbf{e}}_c+\mathbf{B_d}\,\dot{\mathbf{e}}_c+\mathbf{K_d}\,\mathbf{e}_c=-\boldsymbol{F}_{ext}+\boldsymbol{F}_{des} \tag{31}$$

where $\mathbf{e_c}$ is the position error during the contact phase

$$\mathbf{e_c}=\mathbf{x}\text{-}\mathbf{x_{d,c}} \tag{32}$$

where $\mathbf{x_{d,c}}$ is the desired trajectory during the contact.

A vector $\mathbf{n}$ normal to the impact surface is defined. The desired impedance, given by (31), can be written in frame {n} whose origin coincides with the origin of the inertial frame and its attitude coincides with the end-effector's attitude, given by the rotation matrix $\mathbf{R_n}$, whose x-axis coincides with $\mathbf{n}$, see Fig. 2 (b). It is known that,

$$\mathbf{e_c}=\mathbf{R_n^*}\,{}^n\mathbf{e_c},\ \boldsymbol{F}_{ext}=\mathbf{R_n^*}\,{}^n\boldsymbol{F}_{ext},\ \boldsymbol{F}_{des}=\mathbf{R_n^*}\,{}^n\boldsymbol{F}_{des} \tag{33}$$

where ${}^n(\cdot)$ denotes the vector $(\cdot)$ expressed in frame {n} and $\mathbf{R_n^*}=\mathrm{diag}(\mathbf{R_n},\mathbf{R_n})$.

Therefore, the impedance behavior in this frame is

$$\tilde{\mathbf{M}}_\mathbf{d}\,{}^n\ddot{\mathbf{e}}_c+\tilde{\mathbf{B}}_\mathbf{d}\,{}^n\dot{\mathbf{e}}_c+\tilde{\mathbf{K}}_\mathbf{d}\,{}^n\mathbf{e}_c=-{}^n\boldsymbol{F}_{ext}+{}^n\boldsymbol{F}_{des} \tag{34}$$

where

$$\tilde{\mathbf{M}}_\mathbf{d}=\mathbf{R_n^{*T}}\,\mathbf{M_d}\,\mathbf{R_n^*},\ \tilde{\mathbf{B}}_\mathbf{d}=\mathbf{R_n^{*T}}\,\mathbf{B_d}\,\mathbf{R_n^*},\ \tilde{\mathbf{K}}_\mathbf{d}=\mathbf{R_n^{*T}}\,\mathbf{K_d}\,\mathbf{R_n^*} \tag{35}$$

If the gain matrices $\mathbf{M_d}$, $\mathbf{B_d}$ and $\mathbf{K_d}$ are chosen as diagonal matrices with equal diagonal elements, then it can be shown that:

$$\tilde{\mathbf{M}}_\mathbf{d}=\mathbf{M_d},\ \tilde{\mathbf{B}}_\mathbf{d}=\mathbf{B_d},\ \tilde{\mathbf{K}}_\mathbf{d}=\mathbf{K_d} \tag{36}$$

Therefore, (34) can be written as:

$$\mathbf{M_d}\,{}^n\ddot{\mathbf{e}}_c+\mathbf{B_d}\,{}^n\dot{\mathbf{e}}_c+\mathbf{K_d}\,{}^n\mathbf{e}_c=-{}^n\boldsymbol{F}_{ext}+{}^n\boldsymbol{F}_{des} \tag{37}$$

where the external force caused by the contact is modeled by a generalized spring and in frame {n} is given by:

$${}^n\boldsymbol{F}_{ext}={}^n\mathbf{K_e}\,{}^n\mathbf{e_c} \tag{38}$$

Assuming point contact, only forces are developed between the end-effector and the target. If friction is negligible, then only normal to the surface forces are developed. Then, the 6×6 stiffness matrix ${}^n\mathbf{K_e}$ expressed in frame {n} is

$${}^n\mathbf{K_e}=\mathrm{diag}(k_e,0,0,0,0,0) \tag{39}$$

where k_e is the spring's stiffness along the contact direction.

Moreover, the desired force in frame {n} can be chosen as

$${}^n\boldsymbol{F}_{des}=[F_{des}\ 0\ 0\ 0\ 0\ 0]^T \tag{40}$$

where F_{des} is the desired force along the contact direction **n.**

Since the direction of the force $\boldsymbol{F}_{act}$ is chosen such that it minimizes attitude disturbances and the target is cooperative, target attitude dynamics can be neglected. Therefore, the desired error response is derived from the projection of the translational part of (37) (i.e. its 3 first components) on the vector $\mathbf{n}=(1,0,0)^T$, after the substitution of (38)-(40) in (37), and considering the diagonal form of the gain matrices:

$$m_d\,\ddot{e}_{c,n}+b_d\,\dot{e}_{c,n}+(k_d+k_e)e_{c,n}=F_{des} \tag{41}$$

The position error $e_{c,n}$ along the contact direction is

$$e_{c,n}(t)=x_{ch}(t)-x_t(t)+l_0 \tag{42}$$

where x_{ch}, x_t are the chaser's end-effector position and the target's position, respectively, along the direction of the impact, and l_0 is the undeformed spring's length, see Fig. 2(b).

Therefore, the desired trajectory during the contact phase, along the direction of the vector $\mathbf{n}$, is

$$x_{d,c}(t)=x_t(t)-l_0 \tag{43}$$

Since it is desired to avoid controller switching but instead have the same controller, given by (24), during both phases, the error dynamics in both phases are described by the same impedance law, given by (21). This is feasible by setting the same controller matrix gains $\mathbf{M_d}$, $\mathbf{B_d}$ and $\mathbf{K_d}$ in both phases, and by an appropriate selection of (i) the desired trajectory $\mathbf{x_d}$ and (ii) the desired force F_{des}.

To avoid controller switching, the desired trajectory $\mathbf{x_d}$ in (22) is defined as

$$\mathbf{x_d}(t)=\mathbf{x_{d,f}}(t)\frac{|1-\|\boldsymbol{F}_{ext}\|/a_1|}{1+a_1\|\boldsymbol{F}_{ext}\|}+\mathbf{x_{d,c}}(t)\frac{\|\boldsymbol{F}_{ext}\|}{\|\boldsymbol{F}_{ext}\|+a_2} \tag{44}$$

where the parameters a_1 and a_2 are chosen enough large and enough small, respectively, so that $\mathbf{x_d}(t)=\mathbf{x_{d,f}}(t)$ in free-space, i.e. when $\|\boldsymbol{F}_{ext}\|=0$, and $\mathbf{x_d}(t)=\mathbf{x_{d,c}}(t)$ during the contact phase, i.e. when $\|\boldsymbol{F}_{ext}\|\neq 0$.

Note that the desired trajectory $\mathbf{x_d}(t)$ in the contact phase, depends on the target position, see (43). Since the application of the developed controller, (24), requires the knowledge of the acceleration $\ddot{\mathbf{x}}_\mathbf{d}$, the corresponding target's acceleration must be available. This can be measured either with respect to the chaser, knowing the chaser's motion, or using the interaction force and an estimate of the target's mass m_t [14].

The desired force F_{des} must be zero in the free-space phase for zero tracking error, while during the contact phase it must be non-zero, to ensure the contact and according to (21), a non-zero steady state error. Therefore, to avoid desired force switching, F_{des} is defined as

$$F_{des}=\frac{F_d\|\boldsymbol{F}_{ext}\|}{\|\boldsymbol{F}_{ext}\|+a} \tag{45}$$

where F_d is a non-zero parameter setting the desired contact force, and a is an arbitrary parameter of small value. During the free-space phase, the contact force $\boldsymbol{F}_{ext}$ is zero, and therefore F_{des} is also zero. However, during the contact and for small a, F_{des} is about equal to the set value F_d.

The error dynamics of the closed-loop system, along the direction of the contact, is given by (41). For positive parameters m_d, b_d and k_d, the system dynamics is stable and the position error at steady state is:

$$e_{ss,c}=\frac{F_d}{k_d+k_e} \tag{46}$$

To obtain a second order error response, described by ζ_c and $\omega_{n,c}$ at the contact phase, the controller gains m_d, b_d must be selected as

$$m_d=\frac{k_d+k_e}{\omega_{n,c}^2} \tag{47}$$

and

$$b_d=2\zeta_c\,\omega_{n,c}\,m_d \tag{48}$$

Since the same controller parameters are required in both phases, comparison of (29) with (47) and of (30) with (48), yields respectively

$$\zeta_c=\zeta_f\sqrt{\frac{k_d}{k_d+k_e}} \tag{49}$$

and

$$\omega_{n,c}=\omega_{n,f}\sqrt{\frac{k_d+k_e}{k_d}} \tag{50}$$

According to (49)-(50), the response in the contact phase, described by ζ_c and $\omega_{n,c}$, depends on the response in the free-space, given by ζ_f, and $\omega_{n,f}$. Defining a desired position error transient response in the free-space phase (i.e. defining ζ_f and $\omega_{n,f}$) and selecting any positive, finite value of k_d, the controller gains m_d and b_d are computed using (29) and (30), respectively. Choosing an overdamped response (i.e. $\zeta_c>1$) during the contact phase, a continuous impact can be achieved, [12]–[13]. However, since $\zeta_c<\zeta_f$, see (49), this choice will result in an overdamped response in the free-space, which is undesirable, as the response will be slow and inefficient [15]. Therefore, a critically damped or underdamped response in the free-space is usually chosen which according to (49) will result in an underdamped response (i.e. $0<\zeta_c<1$) in the contact phase. Next, the response during the contact phase is studied.

V. Contact Response

In the previous section, we introduced the impedance control law and defined the resulting error dynamics of the closed – loop system in both the free-space and the contact phases. It was shown that the choice of a critically damped or underdamped desired response in the free-space results in underdamped response during the contact phase. In this section, we study this underdamped response and define the sufficient conditions so that the chaser will not lose contact with the target.

During contact, the end-effector deforms the target with an oscillating response, which assuming maintenance of contact, finally reaches a steady state target deformation. In Fig. 3, a typical underdamped response of the end-effector's position error is presented along with some interesting characteristics.

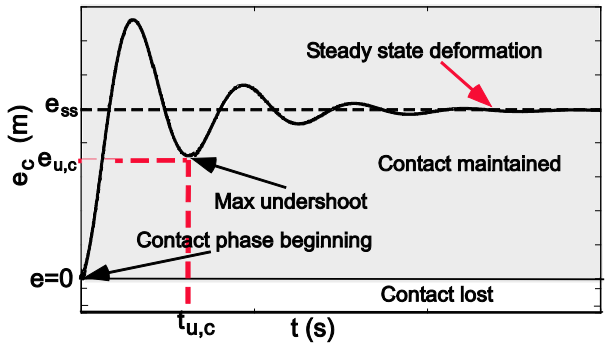

Fig. 3. The underdamped error response of the chaser during the contact.

The position error response of an underdamped system, $0<\zeta_c<1$, with a *non-zero* initial relative velocity of the chaser end-effector, is obtained as the solution of (41) in the form

$$e_{c,n}(t)=\frac{F_d}{k_e+k_d}+A_c\,e^{-\zeta_c\omega_{n,c}t}\sin(\omega_{n,c}\sqrt{1-\zeta_c^2}\,t+\psi_c) \tag{51}$$

where the parameters $\zeta_c,\omega_{n,c}$ are given by (49)-(50), ψ_c is the oscillation phase and the amplitude A_c is given by

$$A_c=\sqrt{\frac{m_d^2\,\omega_{n,c}^2\,v(0)^2-2F_d m_d\,\omega_{n,c}\,\zeta_c\,v(0)+F_d^2}{(k_e+k_d)^2(1-\zeta_c^2)}} \tag{52}$$

where $v(0)$ is the initial value of the chaser's end-effector relative velocity $v(t)$ at the contact phase defined as

$$v(t)=\dot{x}_{ch}(t)-\dot{x}_t(t) \tag{53}$$

To avoid any contact loss with the target, the error $e_{u,c}$ which corresponds to the maximum undershoot, see Fig. 3, must be positive, i.e.

$$e_{u,c}=e_{c,n}(t_{u,c})>0 \tag{54}$$

where $t_{u,c}$ is the time where the maximum undershoot appears, see Fig. 3.

As shown in Fig. 3, the maximum undershoot of the error response can be positive if the amplitude of the response is not large. Therefore, we find the conditions for which the amplitude A_c is minimum, and examine if the undershoot of the response given by (51) is then positive. Using (52), it can be shown that the amplitude A_c is minimum when the chaser's initial relative impact velocity $v(0)$ takes the value

$$v_d=\frac{F_d\,\zeta_c}{m_d\,\omega_{n,c}} \tag{55}$$

The minimum value of the amplitude A_c is then obtained by substituting the relative velocity v_d in (52) to yield

$$A_{c,min}=\frac{F_d}{k_d+k_e} \tag{56}$$

Then, the undershoot of the error response is

$$e_{u,c}=\frac{F_d}{k_d+k_e}(1+e^{-\zeta_c\omega_{n,c}t_{u,c}}\sin(\omega_{n,c}\sqrt{1-\zeta_c^2}\,t_{u,c}-\frac{\pi}{2})) \tag{57}$$

Since the right-hand side of (57) is always positive, one concludes that (54) is satisfied. The above analysis shows that continuous contact of the chaser with the target can be guaranteed if the initial velocity of the chaser at the contact phase is given by (55). This velocity is the terminal chaser's velocity in the free-space phase, and can be achieved by proper design of the desired trajectory, given by (28). To this end, the coefficients of the polynomial $s(t)$ in (28) are selected so that the chaser will arrive at the target at the moment of the contact with relative velocity v_d given by (55).

Example: To illustrate the developed method, a planar chaser with a 3 dof manipulator is employed. The system parameters are shown in Table I. The target, of mass $m_t=100Kg$ and moment of inertia $I_t=50Kgm^2$, is initially at rest at $(x_{t,in}\ y_{t,in})=(2.5\ 2.5)m$ with orientation $\theta_t=0^o$. The chaser's end-effector is driven to the target from an initial position $(x_{ch,in}\ y_{ch,in})=(0.1\ 0.1)m$ with orientation $\theta_{ch,in}=60^o$ to the target's position with final orientation $\theta_{ch,fin}=0^o$ in time $t=100s$. The initial position of the base CoM and the base's orientation are $(x_b\ y_b)=(-2.0\ 0.05)m$ and $\theta_b=0^o$, respectively. The contact between the chaser and the target is modeled by a spring of natural length $l_0=0.1m$ and stiffness

$k_e^* = 10 kN/m$. The control law (24) is applied on the chaser both during the free-space and the contact phases.

Table I. Parameters of the planar chaser.

Body	l_i (m)	r_i (m)	m_i (Kg)	I_i(Kg m^2)
0	-	1.0	400	200
1	1.0	1.0	50	16.67
2	1.0	1.0	50	16.67
3	0.5	0.5	50	4.17

The impedance parameters k_d and the desired force F_d define the steady state position error in the contact phase, according to (46). These are selected as

$$k_d = 100 N/m \ , \ F_d = 0.1 N \tag{58}$$

to achieve a steady state position error about $10^{-5} m$.

The 3×3 diagonal matrices $\mathbf{M_d}$, $\mathbf{B_d}$ and $\mathbf{K_d}$ used in the control law (24) are:

$$\mathbf{M_d} = diag(m_d) \ , \ \mathbf{B_d} = diag(b_d) \ , \mathbf{K_d} = diag(k_d) \tag{59}$$

The impedance parameters m_d , b_d are found considering a desired position error response in the free-space phase. This response is defined by setting the damping coefficient $\zeta_f = 1$ and the natural frequency $\omega_{n,f} = 0.6 rad/s$ during the free-space phase. Using (47) and (48), these are computed as

$$m_d = 277.8 kg \ , \ b_d = 333.3 Ns/m \tag{60}$$

The required chaser's initial velocity in the contact phase which guarantees continuous contact with the target, (55), is

$$v_d = 5.9 \cdot 10^{-6} m/s \tag{61}$$

The position error response along the contact direction, the chaser and target velocities in this direction during the contact, and the corresponding external force are shown in Fig. 4(a). As can be seen, the chaser does not lose contact with the target since the error shown in Fig. 4(a) is always positive. The required joint torques as well as the forces/moments applied on the chaser's base by thrusters and reaction wheels, computed using (25) and displayed in Fig. 4(b) and Fig. 4(c), respectively, are small and smooth, guaranteeing the feasibility of the required task.

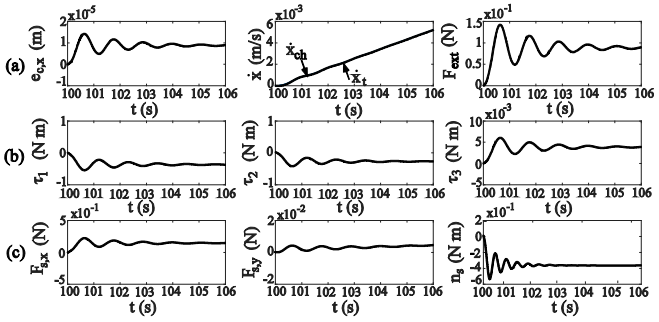

Fig. 4. (a) The position error response along the contact direction, the chaser and target velocities along this direction during contact and the corresponding external force, (b) the applied joint torques and (c) the applied force/ moment on the chaser base during contact.

VI. CONCLUSIONS

In this paper, the problem of obtaining continuous contact between a chaser and its target was studied. The task was divided into the free-space and the contact phase. It was shown that continuous contact between the two moving systems is achieved by the selection of an appropriate chaser velocity at the moment of contact, accompanied by an impedance controller, with its parameters selected such that the same controller can be used throughout both phases. A methodology was developed for selecting the same controller gains for both phases and for designing an accompanying desired trajectory. The method was developed for spatial systems and was illustrated by a planar example.

REFERENCES

[1] Fineberg, L., Treptow, J., Bass, T., Clark, S., Johnson, Y., Poffenberger, B., "A Novel Approach for Controlled Deorbiting and Reentry of Small Spacecraft," *3rd Annual Space Traffic Management Conference, "Emerging Dynamics"*, 2016.

[2] Hogan, N., "Impedance control: An approach to manipulation," *Proc. American Control Conference*, June 1984, pp. 304-313.

[3] Yoshida, K., Nakanishi, H., Ueno, H., Inaba, N., Nishimaki, T., and Oda, M., "Dynamics, control and impedance matching for robotic capture of a non-cooperative satellite," *Advanced Robotics*, Vol. 18, No. 2, 2004, pp. 175-198.

[4] Nakanishi, H., Uyama, N., and Yoshida, K., "Virtual mass of impedance system for free-flying target capture," *IEEE/RSJ International Conference on Intelligent Robots and Systems*, Taipei, 2010, pp. 4101-4106.

[5] Moosavian, S. Ali A. and Papadopoulos, E., "Cooperative object manipulation with contact impact using multiple impedance control" *Int. J. Control, Automation, and Systems*, 8 (2), 2010, pp. 314–327.

[6] Schneider, S.A., Cannon Jr., R.H., "Object impedance control for cooperative manipulation: theory and experimental results," *IEEE Trans. Robotics Automation*, Vol. 8, No.3, 1992, pp. 383-394.

[7] Abiko, S., Lampariello, R., and Hirzinger, G., "Impedance Control for a Free-Floating Robot in the Grasping of a Tumbling Target with Parameter Uncertainty," *IEEE/RSJ Int. Conference on Intelligent Robots and Systems*, Beijing, China, 2006, pp. 1020-1025.

[8] Seweryn, K., Rybus, T., Colmenarejo, P., Novelli, G., Oleś, J., Pietras, M., Sasiadek, J., Z., Scheper, M., Tarenko, K., "Validation of the robot rendezvous and grasping manoeuvre using microgravity simulators," *IEEE International Conference on Robotics and Automation,* May 21-25, 2018, pp. 873-880.

[9] Lampariello, R., Mishra, H., Oumer, N., Schmidt, P., Marco De Stefano, Albu-Schaffer, A., "Tracking Control for the Grasping of a Tumbling Satellite with a Free-Floating Robot," *IEEE Robotics and Automation Letters,* Vol. 3, Issue. 4, 2018, pp. 3638-3645.

[10] Sharma, S., Suomalainen, M., and Kyrki, V., "Compliant Manipulation of Free-Floating Objects," *IEEE International Conference on Robotics and Automation,* May 21-25, 2018, pp. 865-872.

[11] Hirano, D., Kato, H., and Saito, T., "Online Path Planning and Compliance Control of Space Robot for Capturing Tumbling Large Object," *IEEE/RSJ International Conference on Intelligent Robots and Systems*, Madrid, Spain, 2018, pp. 2909-2916.

[12] Uyama, N., Nakanishi, H., Nagaoka, K., and Yoshida, K., "Impedance-Based Contact Control of a Free-Flying Space Robot with a Compliant Wrist for Non-Cooperative Satellite Capture," *IEEE/RSJ International Conference on Intelligent Robots and Systems*, Vilamoura, Algarve, Portugal, 2012, pp. 4477-4482.

[13] Perez, P., R., De Stefano, M., and Lampariello, R., "Velocity Matching Compliant Control for a Space Robot during Capture of a Free-Floating Target," *IEEE Aerospace Conference*, MT, USA, 2018.

[14] Sheinfeld, D., and Rock, S., "Rigid Body Inertia Estimation with Applications to the Capture of a Tumbling Satellite," *19th ASS/AIAA Spaceflight Mechanics Meeting*, Vol. 134, 2009, pp. 343-356.

[15] Nise, N., "Control Systems Engineering," *6th Edition*, *John Willey and Sons, Inc*, 2011.